Pyranose Ring Flexibility. Mapping of Physical Data for Iduronate in Continuous Conformational Space

Steffen Ernst,[‡] Ganesh Venkataraman,[†] V. Sasisekharan,[‡] Robert Langer,[‡,†] Charles L. Cooney,[‡] and Ram Sasisekharan*[,¶]

Contribution from the Department of Chemical Engineering, Harvard−MIT Division of Health Sciences and Technology, and Whitaker College of Health Sciences and Technology, Massachusetts Institute of Technology, Cambridge, Massachusetts 02139

Received July 1, 1997. Revised Manuscript Received October 24, 1997

Abstract: A method for relating pyranose ring conformation to experimental measurements is presented. A three-dimensional conformational space (Q, θ, P_2) based on a torsion angle formalism is projected in two dimensions (θ, P_2) and contours of calculable physical properties are plotted and compared to experimentally determined values. With this approach, conformations in a continuous conformational space that fit the physical data can be identified rapidly and the conformational space available to pyranose rings can be visualized easily. Iduronate, which is part of biologically important glycosaminoglycans such as dermatan sulfate, shows similar stability in several ring conformations. Thus, we find it is desired to extend the conformational analysis from canonical chair and skew-boat conformations to a continuous conformational space, when interpreting biophysical data related to the iduronate ring conformation. When the method is applied to the physical data available for dermatan sulfate, the results indicate that two families of α-L-iduronate conformations each can explain both 2D-NMR and X-ray diffraction data for dermatan sulfate. Further, the mapping technique was used to investigate the interconversion between different conformations of the iduronate residue. The method described here offers a systematic search of conformations beyond the canonical chair, boat, and skew boat conformations and provides a graphical description of the deviations from these ideal conformers. The approach thus can be extended to ring conformational analysis of other pyranoses.

Introduction

The topology of oligo- and polysaccharides is determined by the ring conformations of the individual monosaccharide units and by the torsion angles of the glycosidic bonds. Much research on carbohydrate conformation currently focuses on accurately modeling electrostatic interactions, hydrogen bonds, and anomeric effects to predict the conformation from force-field-based energy calculations.[1, 2] Often, experimentally measurable properties can be explained by the global minimum structure, or by the time-average of several structures based on a Boltzman distribution or molecular dynamics calculation.[3, 4] These force field based approaches have favored the use of Cartesian coordinates in modeling pyranoses; however, in some cases this may not be optimal for describing ring conformation and flexibility. Here we investigate an alternative approach to analyzing experimental data related to pyranose ring conformation. The conformational search is biased toward the data themselves by reducing the energy calculations to simply ensuring that the conformations are stereochemically accessible, and a torsion angle based approach[5] is invoked to describe pyranose ring conformation. Iduronate from the glycosaminoglycan dermatan sulfate is used as the model system for this methodology.

The problem of assigning ring conformation for six-membered rings such as pyranoses has long been recognized. On the basis of the configuration of hydroxyl and carboxylate groups of pyranose rings, it can be estimated which of the two chair forms, $^4C_1$ and $^1C_4$, is more stable.[6] Fourteen of the sixteen aldohexopyranoses have more bulky exocyclic groups oriented equatorially in one form compared to the other, and are therefore predicted to be found exclusively in that conformation ($^4C_1$ for D-forms, $^1C_4$ for L-forms).[6] Only α-idose and α-altrose show similar stability of $^4C_1$ and $^1C_4$ conformations based on the equatorial/axial orientation of the exocyclic groups. Consequently, the assignment of ring conformation for α-L-iduronate has led to discussion.[7, 8] Force-field-based molecular modeling and biophysical experiments have been invoked to address this issue for dermatan sulfate (Figure 1) a polysaccharide with a repeat unit of *N*-acetylated-D-galactosamine-(β1,4)-D-glucuronic acid, which is modified by 4-*O*-sulfation of the galactosamine (abbreviated $Gal_{NAc,4S}$) and epimerization of β-D-glucuronic acid to α-L-iduronic acid (abbreviated IdoA). Both reactions most often proceed to 80−95% conversion.[9] Energy minimizations indicated very similar energy of the $^1C_4$, $^4C_1$, and ^2S_O conforma-

* To whom correspondence should be addressed at MIT, 77 Massachusetts Avenue, Building E18-568, Cambridge, Massachusetts 02139.
‡ Department of Chemical Engineering.
† Harvard-MIT Division of Health Sciences and Technology.
¶ Whitaker College of Health Sciences and Technology.

(1) Pérez, S.; Imberty, A.; Carver, J. P. *Adv. Comput. Biol.* **1994**, *1*, 147−202.
(2) French, A. D.; Brady, J. W. *ACS Symp. Ser.* **1990**, *430*, 1−19.
(3) Engelsen, S. B.; Pérez, S.; Braccini, I.; du Penhoat, C. H. *J. Comput. Chem.* **1995**, *16*, 1096−1119.
(4) Forster, M. J.; Mulloy, B. *Biopolymers* **1993**, *33*, 575−588.
(5) Haasnoot, C. A. G. *J. Am. Chem. Soc.* **1992**, *114*, 882−887.
(6) Stoddart, J. F. *Stereochemistry of Carbohydrates*; John Wiley and Sons: New York, 1971.
(7) Casu, B.; Choay, J.; Ferro, D. R.; Gatti, G.; Jacquinet, J. C.; Petitou, M.; Provasoli, M.; Ragazzi, M.; Ferro, D. R.; Sinaÿ, P.; Torri, G. *Nature* **1986**, *322*, 215−216.
(8) Rees, D. A.; Morris, E. R.; Stoddart, J. F.; Stevens, E. S. *Nature* **1985**, *317*, 480.

S0002-7863(97)02185-9 CCC: $15.00
Published on Web 02/20/1998

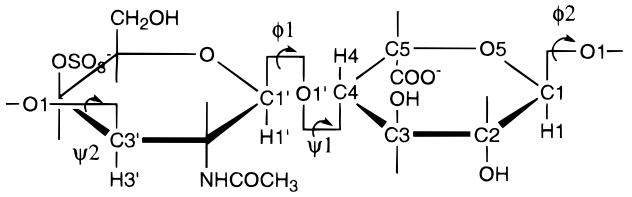

Figure 1. The disaccharide repeat of dermatan sulfate, 4-*O*-sulfate *N*-acetyl-β-D-galactosamine-(1,4)-α-L-iduronic acid-(1,3). The interresidue torsion angles ϕ_1, ψ_1, ϕ_2, and ψ_2 are shown. The nomenclature of the ring atoms of iduronate used for description of ring puckering and torsion angles is shown, thus, for example, ϕ_{C1C2} is the O5−C1−C2−C3 torsion.

tions of iduronate.[10,11] Also, experimental results have led to conflicting interpretations in terms of the α-L-iduronate ring conformation. Three different helix symmetries of dermatan sulfate (2_1, 3_1, and 8_3) have been calculated from X-ray diffraction patterns.[12−14] All three have long helix repeats, which were interpreted to indicate a $^4C_1$ conformation of the iduronate.[12] Low proton−proton coupling constants, however, suggested a $^1C_4$ conformation of the iduronate.[15, 16] Dermatan sulfate is highly susceptible to periodate oxidation, which is believed to indicate that the O2−O3 enolate group must be gauche, consistent with a $^4C_1$ or ^2S_O but not with a $^1C_4$ conformation.[17] However, this interpretation of periodate oxidation data has been questioned by Rees and co-workers, who maintain that a dynamic equilibrium between a gauche and a trans conformation (with respect to the O2−O3 enolate) can explain the periodate data, even if only a small subset of the iduronic acid residues are in the gauche conformation.[8] Crystal structures show that iduronate can attain $^1C_4$, $^4C_1$, or ^2S_O conformations when present in oligosaccharides that are bound to basic fibroblast growth factor.[18,19] Considering that variations in physical conditions among experiments may result in different structures for each experiment, it is desired to corroborate all these results into a consistent picture of the conformational behavior of iduronate in dermatan sulfate.

In an earlier contribution, we also relied on an energy criterion based exclusively on eliminating bad steric contacts,[20] thus extending the conformational analysis beyond the global minimum to the "stereochemically accessible domain". We searched the entire range of iduronate conformations by driving three of the endocyclic torsion angles and the four interresidue torsions ($\phi1$, $\psi1$, $\phi2$, and $\psi2$), selecting for conformations that would satisfy diffraction data for dermatan sulfate and ring closure criteria without nonbonded overlap.[20] This analysis showed that of four stereochemically accessible conformations for α-L-iduronate ($^1C_4$, $^4C_1$, $^OS_2$, and ^2S_O), only three satisfied the X-ray diffraction criteria ($^4C_1$, $^OS_2$ and ^2S_O).[20] Searching conformational space by energy minimization approaches leads to results that may be quite force-field dependent.[3] We find that the approach of considering the entire stereochemically accessible domain for conformations that satisfy experimental data reduces this problem of force-field dependence of the calculations.

The conformational space for pyranose rings has been described as a sphere, first by Hendrickson,[21] and then in a more explicit form, generalized to any six-membered ring, by Cremer and Pople.[22] This description is valuable for visualizing the interrelationship of chair, boat, skew-boat, and other canonical conformations, and for explicitly describing model and observed structures without providing atomic coordinates. However, calculation of internal atomic coordinates for a given point in the Cremer−Pople sphere is complicated, which may have limited the use of this formalism. Recently, Haasnoot described a similar formalism for six-membered rings, which is based on internal torsion angles.[5] This formalism facilitates calculation of internal coordinates for a given point in the spherical ring conformation space.

Here we describe a continuous graphical approach to analyzing pyranose ring flexibility. Physical properties are related to the conformational space available to iduronate, using the torsion-based formalism for description of six-membered rings.[5,23] Contrary to conventional approaches to ring conformational analysis, we focus on a stereochemically accessible domain in conformational space, rather than on minimized conformations. This approach offers a systematic search to fit experimental data for conformations beyond the canonical chair, boat, and skew-boat conformations, and we find that it provides an informative graphical description of the deviations from ideality. In the case of dermatan sulfate, we identified conformations that satisfy the apparently contradictory experimental data.

Methods

To describe the conformational space for the six-membered iduronate ring, we used the spherical coordinates (radius Q, azimuthal θ, and meridian P_2) introduced by Haasnoot,[5] which are related to endocyclic torsion angles by a truncated Fourier series (eqs 7−10 from Haasnoot[5]). Due to the requirement of closing the ring with reasonable bond lengths and bond angles, the conformational space is a flattened shell, which was approximated by an ellipsoid: $Q = 55 + 10(\sin\theta)$. The spherical coordinates were used as drivers for exploring physical properties of the conformational space for iduronate. At each grid point (θ, P_2), we calculated Q and the endocyclic torsion angles for a homocyclic ring.

Physical properties, in turn, were calculated from these conformational parameters. The proton−proton torsion angle (ϕ_{HH}) is equal to the endotorsion ($C_{i-1}-C_i-C_{i+1}-C_{i+2}$) plus a constant, which is independent of the ring conformation. The constants 118°, −118°, 118°, and 0° were used for the $\phi_{H1,H2}$, $\phi_{H2,H3}$, $\phi_{H3,H4}$, and $\phi_{H4,H5}$ proton−proton torsion angles, respectively.[23] The coupling constants, $^3J_{HH}$, were estimated from the proton−proton torsion angle (ϕ_{HH}) for α-L-iduronate by using the Karplus−Altona equation, corrected for electronegativity (eqs 8 and 9 from Haasnoot[24] with electronegativity values from Huggins[25]). A later parametrization of the Haasnoot equation, based on empirical electronegativities, has been introduced,[26] but the substituent groups found in pyranoses were not included in the tables of group electronegativities provided, so we chose to proceed with the

(9) Ernst, S.; Langer, R.; Cooney, C. L.; Sasisekharan, R. *CRC Crit. Rev. Biochem. Mol. Biol.* **1995**, *30*, 387−444.
(10) Ragazzi, M.; Ferro, D. R.; Provasoli, A. *J. Comput. Chem.* **1986**, *7*, 105−112.
(11) Dowd, M. K.; French, A. D.; Reilly, P. J. *Carbohydr. Res.* **1994**, *264*, 1−19.
(12) Mitra, A. K.; Arnott, S.; Atkins, E. D. T.; Isaac, D. H. *J. Mol. Biol.* **1983**, *169*, 873−901.
(13) Arnott, S.; Guss, J. M.; Hukins, D. W. L.; Mathews, M. B. *Biochem. Biophys. Res. Commun.* **1973**, *54*, 1377−1383.
(14) Atkins, E. D. T.; Isaac, D. H. *J. Mol. Biol.* **1973**, *80*, 773−779.
(15) Gatti, G.; Casu, B.; Torri, G.; Vercelotti, J. R. *Carbohydr. Res.* **1979**, *68*, C3−C7.
(16) Winter, W. T.; Taylor, M. G.; Stevens, E. S.; Morris, E. R.; Rees, D. A. *Biochem. Biophys. Res. Commun.* **1986**, *137*, 87−93.
(17) Scott, J. E.; Tigwell, M. J. *Biochem J.* **1978**, *173*, 103−114.
(18) Ornitz, D. M.; Herr, A. B.; Nilsson, M.; Westman, J.; Svahn, C.-M.; Waksman, G. *Science* **1995**, *268*, 432−436.
(19) Faham, S.; Hileman, R. E.; Fromm, J. R.; Linhardt, R. J.; Rees, D. C. *Science* **1996**, *271*, 1116−1120.
(20) Venkataraman, G.; Sasisekharan, V.; Cooney, C. L.; Langer, R.; Sasisekharan, R. *Proc. Natl. Acad. Sci. U.S.A.* **1994**, *91*, 6171−6175.
(21) Hendrickson, J. B. *J. Am. Chem. Soc.* **1967**, *89*, 7047−7061.
(22) Cremer, D.; Pople, J. A. *J. Am. Chem. Soc.* **1975**, *97*, 1354−1358.
(23) Haasnoot, C. A. G. *J. Am. Chem. Soc.* **1993**, *115*, 1460−1468.
(24) Haasnoot, C. A. G.; de Leeuw, F. A. A. M.; Altona, C. *Tetrahedron* **1980**, *36*, 2783−2792.
(25) Huggins, M. L. *J. Am. Chem. Soc.* **1953**, *75*, 4123−4126.
(26) Altona, C.; Francke, R.; de Haan, R.; Ippel, J. H.; Daalmans, G. J.; Westra Hoekzema, A. J. A.; van Wijk, J. *Magn. Res. Chem.* **1994**, *32*, 670−78.

original parametrization.[24] (Using the new parametrization with estimated values of the missing group electronegativities[27] did not change the results significantly.) For each grid point of the conformational mapping, we calculated the four coupling constants and the root-mean-square (rms) of the difference between these and the coupling constants observed for dermatan sulfate.[15] Also, for each grid point, the internal Cartesian coordinates for iduronate were generated by using the average bond lengths and bond angles for carbohydrates[28] and the appropriate rotation matrixes.[29] Values for internal distances and torsion angles were used without further refinement of the structures. The spherical surface that represents the pyranose pucker conformational space was projected in two dimensions as $x = \theta \cos(P_2)$ and $y = \theta \sin(P_2)$ for $\theta \leq 90°$, and $x = (180° - \theta) \cos(P_2)$ and $y = (180° - \theta) \sin(P_2)$ for $\theta \geq 90°$, and the calculated values of physical data (rms of the fit to experimental $^3J_{HH}$ values) and geometric properties (O1−O4 distance and eclipsed endotorsion angles) were contoured by using MATLAB (MathWorks, Natick, MA). Importantly, conversion between Cartesian and spherical coordinates requires numeration of the atoms. According to IUPAC recommendations, the ring oxygen is atom number 1, ring carbon 1 is atom number 2, etc., thus, a $^1C_4$ conformation of a carbohydrate (D or L), which has ring carbon 1 above the plane and ring carbon 4 below the plane, corresponds to a $^2C_5$ chair (atom number 2 above the plane and atom number 5 below the plane) in the generalized notation of Haasnoot, which due to symmetry is identical to $^4C_1$ in the diagrams shown in Haasnoot's article.[5] In the following, the conformations $^1C_4$, $^4C_1$, etc. refer to the traditional carbohydrate nomenclature. The skew-boat forms are denoted ^2S_O, $^OS_2$, etc. (according to IUPAC recommendations) as opposed to the ^2T_O, $^OT_2$, etc. used by Haasnoot.[5] The spherical coordinates of the Haasnoot formalism are closely related to those of Cremer and Pople.[22] The azimuthal angles are approximately equal, and in the Haasnoot formalism, the meridian, P_2, is shifted about 30° higher compared to ϕ_2 of the Cremer−Pople formalism except for ring conformations located close to the poles, where this difference in the meridian can deviate considerably from 30°. Deviations from this correlation between Haasnoot and Cremer−Pople coordinates appear to be unsystematic.

Explicit molecular models were built for selected conformations by using the Insight II and Discover molecular simulation packages (version 95.0 Molecular Simulations, San Diego, CA). For *N*-acetylgalactosamine and for iduronate in $^1C_4$, $^4C_1$, and ^2S_O forms, starting conformations were taken from the literature.[12,30] These conformations were minimized by using 500 steps of the Newton−Raphson algorithm and the Amber force field[31,32] without electrostatic contributions. Then the five exotorsions were each varied in three steps to cover all combinations of staggered conformations, and the least-energy conformation was selected and minimized again. For noncanonical structures that corresponded well to experimental data and for $^OS_2$, starting conformations were found from the spherical coordinates, and adjusted to account for the heterocyclic oxygen by varying bond angles and bond lengths within experimentally observed ranges,[28] and by adjusting torsion angles slightly, not to move away from the starting point in θ,P_2 space. The resulting conformations were minimized as described above, except that a torsion term was introduced to force the ring to remain close to the starting conformation (force constant = 50 kcal mol^{-1} rad^{-2}). $^3J_{HH}$ coupling constants were calculated for the minimized structures, as described above.

Also $^3J_{CH}$ and $^2J_{CC}$ couplings were predicted from the minimized structures. $^3J_{CH}$ couplings for C−O−C−H segments are correlated to the torsion angle ϕ_{COCH} as $^3J_{CH} = 5.7 \cos^2(\phi_{COCH}) - 0.6 \cos(\phi_{COCH}) + 0.5$.[33] For the two C−O−C−H torsions in the iduronate ring (C5−O5−C1−H1 and C1−O5−C5−H5), this formula was used to calculate the corresponding coupling constants ($^3J_{C5H1}$ and $^3J_{C1H5}$). Two-bond $^{13}C-^{13}C$ coupling constants for C−C−C segments can be correlated to the pattern of electronegative substituents relative to the coupled atoms.[34] The pattern of substituents is expressed as a projection sum.[34,35] From the data of Church et al.,[34] this projection sum (P) was related to the two-bond coupling constant ($^2J_{C1,C3}$ and $^2J_{C2,C4}$) by linear regression, which resulted in the following expressions: $^2J_{C1,C3} = -1.6 + 2.5P_{(C1,C3)}$ and $^2J_{C2,C4} = -3.0 + 2.3P_{(C2,C4)}$. It is only possible to measure the absolute value of the coupling constants. Church et al. assigned the signs of measured coupling constants based on knowledge of the structures,[34] but for the predictions made here, a difference in sign cannot be measured and hence is of no consequence. Importantly, the correlations for $^3J_{CH}$ and for $^2J_{C,C}$ are derived from much less data than the correlation for $^3J_{HH}$ couplings.[24] As a consequence, predicted $^3J_{CH}$ and $^2J_{C,C}$ values are expected to be less accurate than predicted $^3J_{HH}$ values.

For a given minimized ring conformation, the stereochemically accessible domain for the glycosidic torsions was found from the $\phi1,\psi1$- and $\phi2,\psi2$-maps, as the area where the nonbonded energy was less than 5 kcal/mol (arbitrarily chosen). The purpose of creating these maps was to *exclude* inaccessible conformations from consideration and not to predict the most likely conformations within the accessible domain. The torsions $\phi1$ and $\psi1$ are defined as (H1′−C1′−O1′−C4) and (C1′−O1′−C4−H4), and $\phi2$ and $\psi2$ as (H1−C1−O1−C3′) and (C1−O1−C3′−H3′), as shown in Figure 1. The ϕ,ψ-maps were generated for a rigid pentasaccharide (IdoA-Gal$_{NAc,4S}$-IdoA-Gal$_{NAc,4S}$-IdoA), using 10° step size and the Amber force field parametrized for carbohydrates[31,32] (version 1.5, Molecular Simulations), which we modified to include sulfate and sulfamate groups.[36] Separate maps were generated for $\phi1,\psi1$ and for $\phi2,\psi2$, and in each case, the other set of torsions were kept fixed at values close to the center of the stereochemically accessible domain. For each grid point, the exocyclic torsions to the acetylate of galactosamine and the carboxylate of iduronic acid (in the case of $\phi1,\psi1$) or to the 4-*O*-sulfate and C6 groups of galactosamine (in the case of $\phi2,\psi2$) were allowed to each sample three different staggered conformations, and the minimum nonbonded energy was chosen.

The relationship between the backbone bond lengths, bond angles, and torsion angles of a periodic polymer, and the resulting helix parameters n (number of disaccharide residues per helix repeat unit) and h (the axial rise per disaccharide residue) were calculated with the FORTRAN program NANDH.[37,38] Values for interresidue torsions were varied in steps of 10°, and sets of torsions that both correspond to the observed helix symmetry (±0.05 Å for n; ±0.1 Å for h) and fall within the stereochemically accessible domain determined by ϕ,ψ-maps were selected. Periodic polymers of dermatan sulfate disaccharides were built for a given set of interresidue and endotorsions, to verify that they are stereochemically accessible.

Results and Discussion

Graphical Representation of Conformational Space. The spherical representation of pyranose conformational space was projected in two-dimensions (θ, P_2), to facilitate plotting of calculated physical properties in a continuous space. A representative plot of the θ,P_2 conformational space is shown in Figure 2, illustrating the location of canonical chair, boat, skew-boat, envelope, and half-chair conformations on the projected sphere. This projection maintains equidistance in the θ direction, while the two-dimensional representation overestimates distances in the P_2 direction by a factor of $\theta/\sin\theta$.

(27) Altona, C.; Ippel, J. H.; Westra Hoekzema, A. J. A.; Erkelens, C.; Groesbeek, M.; Donders, L. A. *Magn. Res. Chem.* **1989**, *27*, 564−576.
(28) Arnott, S.; Scott, W. E. *J. Chem. Soc., Perkin. Trans.* **1972**, *2*, 324−335.
(29) Mortenson, M. E. *Geometric Modeling*; John Wiley: New York, 1985.
(30) Mulloy, B.; Forster, M. J.; Jones, C.; Davies, D. B. *Biochem. J.* **1993**, *293*, 849−858.
(31) Weiner, S. J.; Kollman, P. A.; Nguyen, D. T.; Case, D. A. *J. Comput. Chem.* **1986**, *7*, 230−252.
(32) Homans, S. W. *Biochemistry* **1990**, *29*, 9110−9118.
(33) Tvaroska, I.; Hricovini, M.; Petrakova, E. *Carbohydr. Res.* **1989**, *189*, 359−362.
(34) Church, T.; Carmichael, I.; Serianni, A. S. *Carbohydr. Res.* **1996**, *280*, 177−186.
(35) Bock, K.; Pedersen, C. *Acta Chem. Scand.* **1977**, *B31*, 354−358.
(36) Huige, C. J. M.; Altona, C. *J. Comput. Chem.* **1995**, *16*, 56−79.
(37) Pattabiraman, N. *NANDH Program*, Ph.D. Thesis, Indian Institute of Science, Bangalore, India, 1979.
(38) Sugeta, H.; Miyazawa, T. *Biopolymers* **1967**, *5*, 673−679.

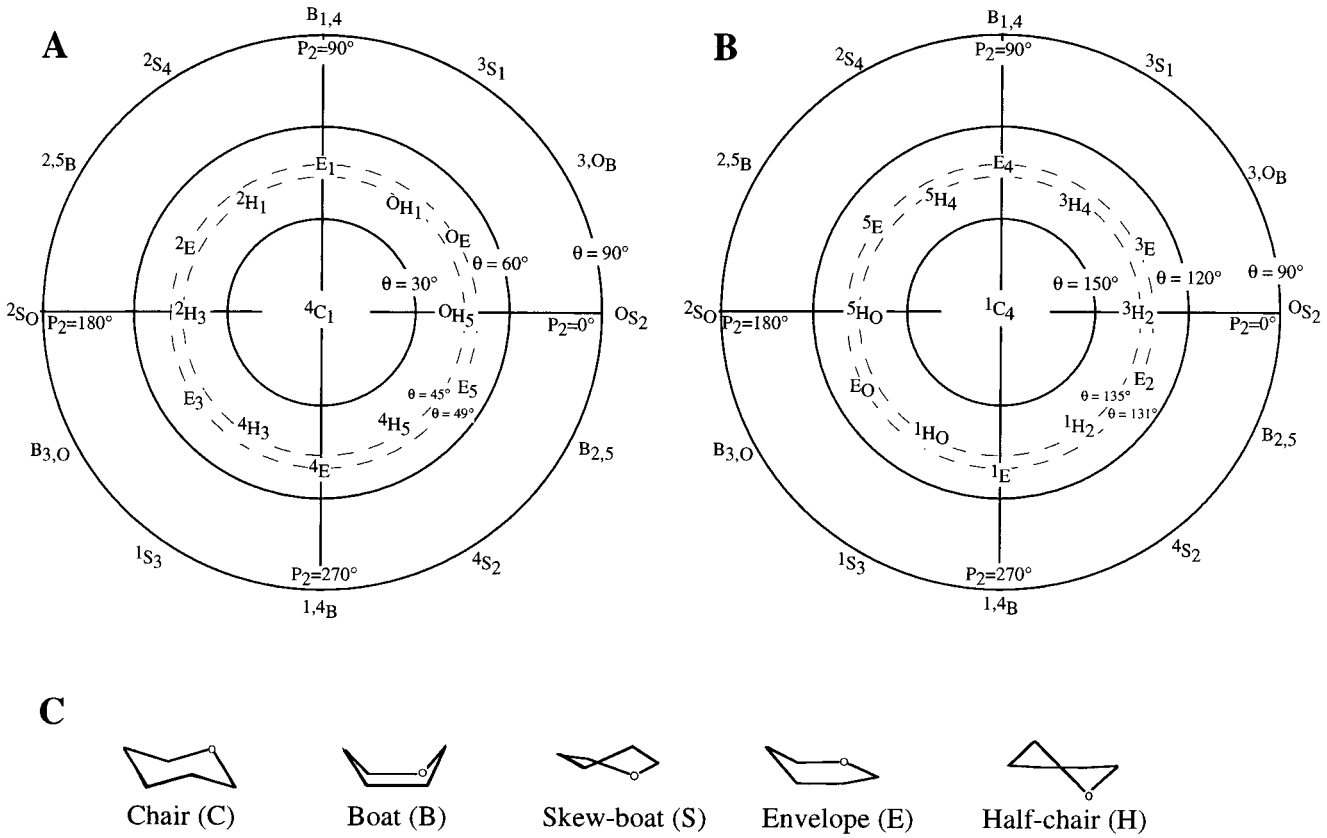

Figure 2. Two-dimensional projection of pyranose ring conformational space. The spherical surface is divided into two hemispheres: Northern for $\theta \leq 90°$ (A) and Southern for $\theta \geq 90°$ (B), with the poles located in the center and the equator at the perimeter of each plot. The $^4C_1$ conformation is at the North pole and the $^1C_4$ at the South pole, and the canonical boat and skew-boats are indicated at the equator of both plots. Envelopes (θ = 49.1° and 130.9°) and half-chairs (θ = 45° and 135°) are located between the poles and the equator. Representative structures of chair, boat, skew-boat, envelope, and half-chair forms are shown (C).

Thus, the representation is most accurate at the center of the plot, where the canonical chair forms that are often observed for carbohydrates are located, and least accurate at the equator ($\theta = 90°$). Ring closure can be optimized for each value of θ and P_2 by varying Q, but using the ellipsoidal approximation for calculating Q as a function of θ (see Methods) conserves the reproducibility of the mapping technique. We found that choosing spherical approximations with Q values in the 50−65° range did not significantly change the results for relating ring conformation expressed solely in θ and P_2 to NMR data.

It can be debated how to best describe various domains within the pyranose conformational space. The frequent use of $^1C_4$, $^4C_1$, and ^2S_O implies that these are singular conformations, while the most illustrative way to describe the domains may be as "$^1C_4$-like" or "$^4C_1$-like", to indicate that each of these is a group of similar conformations. For each of the conformations reported as $^1C_4$, ^2S_O, etc. by different groups, there are often differences in the exact conformation, manifested in the variability of the calculated coupling constants.[20,30,39] This may reflect differences in the methods of generating model structures of each laboratory. Also, "distorted $^1C_4$" structures have been reported, along with calculated physical properties.[16,39] A distorted $^1C_4$ conformation is a deviation from the local $^1C_4$ minima. From the reports, it can be unclear how the $^1C_4$ conformation is distorted,[39] or if it is distorted in a similar or different fashion than other "distorted $^1C_4$".[40] Consequently, we find that there is a need for a method for explicit, informative description of model and observed structures of sugar puckers, short of providing Cartesian coordinates. The torsion angle formalism[5] and its graphical projection presented in this paper represent such a method.

Mapping of NMR Data in the Conformational Space. Using this representation of the pyranose pucker conformational space, we mapped the agreement between α-L-iduronic acid ring conformations and the experimentally observed coupling constants for dermatan sulfate,[15] expressed as rms of the difference between calculated and experimental coupling constants (Figure 3). Structures ***a*** ($\theta \approx 110°$, $P_2 \approx 190°$), ***b*** ($\theta \approx 170°$, $P_2 \approx 350°$), and ***c*** ($\theta \approx 90°$, $P_2 \approx 330°$) on the "Southern" hemisphere are the conformations that individually satisfy the coupling constants best. No conformer on the "Northern" hemisphere has rms lower than 2, and thus no "$^4C_1$-like" conformers can individually satisfy the NMR data. For structure ***c***, which corresponds to a $B_{2,5}$ form, steric overlap between C6 and O2 could not be eliminated, but the other two conformations were stereochemically accessible. Minimized molecular models of conformations ***a*** and ***b***, which each represent an area in conformational space, are shown in Figure 4. Minimization changes the properties only slightly from the symmetrical structures used for calculation of $^3J_{HH}$ for the contour plot (Figure 3). The minimized conformations ***a*** and ***b*** fit experimental data to within 0.6 and 0.8 Hz, respectively. The Karplus−Altona equation was regressed to experimental data with an rms of 0.48 Hz.[24] $^3J_{23}$ of dermatan sulfate is 6.0 Hz, which is in a range (5.5−7.0 Hz) that is very poorly represented in the sample of experimental data used for regression.[24]

(39) Rao, V. S. R.; Balaji, P. V.; Qasba, P. K. *Glycobiology* **1995**, *5*, 273−279.

(40) Torri, G.; Casu, B.; Gatti, G.; Petitou, M.; Choay, J.; Jaquinet, J. C.; Sinaÿ, P. *Biochem. Biophys. Res. Commun.* **1985**, *128*, 134−140.

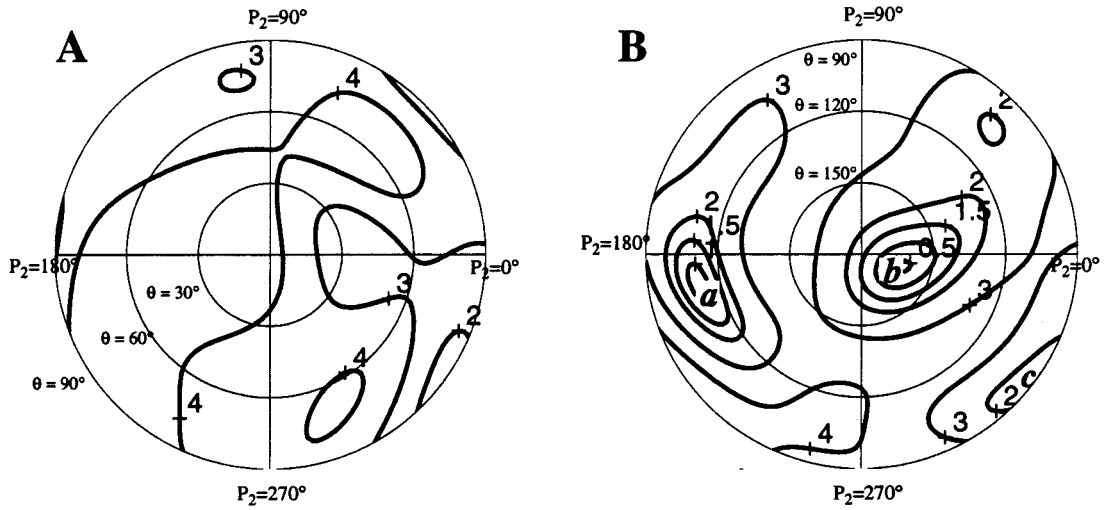

Figure 3. Mapping of $^3J_{HH}$ in iduronic acid ring conformational space. For each point in the conformational space, the four $^3J_{HH}$ coupling constants were calculated as described, and the root mean square (rms) of the difference between calculated and experimentally observed coupling constants for dermatan sulfate[15] was determined. This rms is contoured at values of 0.5, 1, 1.5, 2, 3, and 4, in a 2D-projection of the conformational space, similar to Figure 2 (Figure 3A is the Northern and Figure 3B the Southern hemisphere). Structures *a*, *b*, and *c* are located in wells of these rms contours, and thus represent conformations that individually satisfy the coupling constants best.

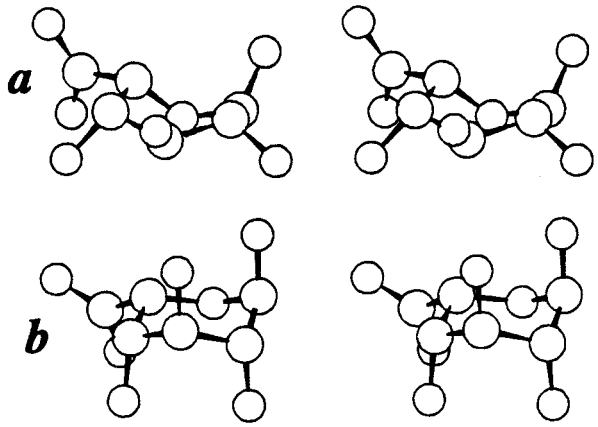

Figure 4. Stereoview of the minimized structures ***a*** and ***b***. For clarity, hydrogens are not shown. The picture was generated by using Insight II (Molecular Simulations, San Diego, CA).

Further, the compounds used for regression[24] were exclusively monomers, while dermatan sulfate is a polysaccharide. These observations, taken together, suggest that the expected deviation of the Karplus−Altona equation for dermatan sulfate will be higher than 0.48 Hz, and that ***a*** and ***b*** are in good agreement with the experimental data, thus supporting a single-state model for the α-L-iduronate conformation in dermatan sulfate. From this analysis, it can be concluded that at least two model structures within the stereochemically accessible domain can individually satisfy the NMR data for dermatan sulfate. Geometrically, ***a*** is "^2S_O-like" and ***b*** is "$^1C_4$-like", but the fit to the NMR data is significantly better for these two structures than for the canonical ^2S_O and $^1C_4$ (Table 1).

The two model structures ***a*** and ***b*** are expected to behave differently with respect to periodate oxidation. Structure ***a*** has the O2−O3 enolate group equatorial and a short (2.9 Å) O2−O3 distance, indicating susceptibility to periodate oxidation, consistent with experimental observations for dermatan sulfate. In contrast, structure ***b*** has the enolate group axial (Table 1).

Also $^2J_{CC}$ and $^3J_{CH}$ couplings have been correlated to conformational parameters,[33−35,41] and experimental values for these parameters can potentially be used to discriminate between structure ***a*** and ***b***. Unfortunately, however, such data are to our knowledge not available for dermatan sulfate. From the minimized structures of α-L-iduronic acid in ***a***, ***b***, $^1C_4$, $^4C_1$, ^2S_O, and $^OS_2$ conformations, estimates of three-bond C−H ($^3J_{C5H1}$ and $^3J_{C1H5}$) and two-bond C−C ($^2J_{C1,C3}$ and $^2J_{C2,C4}$) coupling constants were calculated as described.[33, 34] These values are reported in Table 2 along with distances between H1 and H3 and between H2 and H5 of the iduronate ring, which may for some ring conformations result in intraring NOE cross-peaks.[42] From Table 2, it is clear that $^3J_{CH}$ values cannot be used to distinguish between ***a***, ***b***, $^1C_4$, and ^2S_O. Further, the absolute values of $^2J_{CC}$ are very close for ***a*** and ***b***, but they could potentially be used to distinguish $^1C_4$ from ^2S_O, since these two conformations show a difference in $^2J_{CC}$ values of about 1 Hz. Finally, the differences in H1−H3 and in H2−H5 distances for iduronic acid in conformation ***a*** and ***b*** are predicted to result in measurable differences in NOE values. Therefore, these calculations suggest that NOE measurements, but not $^3J_{CH}$ or $^2J_{CC}$ measurements, could be used to distinguish between the two conformations, ***a*** and ***b***, in dermatan sulfate.

An alternative explanation of the NMR data for dermatan sulfate has been suggested.[43,44] It invokes the existence of a dynamic equilibrium between two or more families of conformations, with the observed coupling constants reflecting a time-average of the coupling constants for these conformers. For comparison, we evaluated how good a fit could be obtained by a simple weighted average of pairs of canonical conformations. Model structures for each of the four conformers ($^1C_4$, $^4C_1$, ^2S_O, and $^OS_2$) that have been invoked in the literature[20,44] were built, and the coupling constants for each conformer calculated, as described above (Table 1). The best fit to the NMR data was found for weighted averages of $^1C_4$ (57−73%) with $^4C_1$ or ^2S_O (27−43%), which give values of coupling constants that compare to the experimental values with an rms difference of

(41) Podlasek, C. A.; Wu, J.; Stripe, W. A.; Bondo, P. B.; Serianni, A. S. *J. Am. Chem. Soc.* **1995**, *117*, 8635−8644.

(42) Mikhailov, D.; Mayo, K. H.; Vlahov, I. R.; Toida, T.; Pervin, A.; Linhardt, R. J. *Biochem. J.* **1996**, *318*, 93−102.

(43) Ferro, D. R.; Provasoli, A.; Ragazzi, M.; Torri, G.; Casu, B.; Gatti, G.; Jacquinet, J.-C.; Sinaÿ, P.; Petitou, M.; Choay, J. *J. Am. Chem. Soc.* **1986**, *108*, 6773−6778.

(44) Ferro, D. R.; Provasoli, A.; Ragazzi, M.; Casu, B.; Torri, G.; Bossennec, V.; Perly, B.; Sinaÿ, P.; Petitou, M.; Choay, J. *Carbohydr. Res.* **1990**, *195*, 157−167.

Table 1. Conformational Parameters and Calculated Coupling Constants for Model Structures of α-L-Iduronate[a]

	Haasnoot			Cremer−Pople			coupling constants (Hz)					distance (Å)	
structure	θ	P_2	Q	θ	ϕ	Q	J_{12}	J_{23}	J_{34}	J_{45}	rms	O2−O3	O1−O4
a	106°	186°	59°	102°	155°	0.66	2.4	7.0	3.2	3.6	0.6	2.94	4.96
b	171°	310°	56°	168°	297°	0.57	3.7	5.0	3.5	2.3	0.8	3.69	4.57
$^1C_4$	173°	185°	55°	175°	134°	0.55	2.5	3.0	3.3	1.1	1.9	3.63	4.53
$^4C_1$	3°	32°	57°	0°	318°	0.57	7.8	9.2	9.1	4.9	4.1	2.86	5.51
^2S_O	93°	180°	65°	90°	148°	0.75	5.2	9.9	5.0	4.1	2.4	2.80	5.08
$^OS_2$	91°	4°	63°	92°	332°	0.73	1.0	5.1	1.2	8.7	3.1	3.65	5.14
73% $^1C_4$, 27% $^4C_1$		N.A.			N.A.		3.9	4.7	4.9	2.1	1.2	N.A.	
57% $^1C_4$, 43% ^2S_O		N.A.			N.A.		3.7	6.0	4.0	2.4	0.6	N.A.	
dermatan sulfate[15]		N.A.			N.A.		3.0	6.0	3.5	3.3	N.A.	N.A.	

[a] Structures ***a*** and ***b*** are described in the text. The canonical $^1C_4$, $^4C_1$, ^2S_O, and $^OS_2$, as well as two examples of weighted averages of these canonical conformations, are included for comparison.

Table 2. Predicted Two-Bond and Three-Bond Coupling Constants and Intraring Hydrogen Distances for α-L-Iduronate in Conformations ***a*** and ***b*** (Described in the Text), as Well as in the Canonical Conformations $^1C_4$, $^4C_1$, ^2S_O, and $^OS_2$[a]

structure	$^3J_{C5H1}$ (Hz)	$^3J_{C1H5}$ (Hz)	$^2J_{C1,C3}$ (Hz)	$^2J_{C2,C4}$ (Hz)	H1−H3 distance (Å)	H2−H5 distance (Å)
a	6.6	6.4	2.2	3.1	3.3	2.8
b	6.8	6.7	(−)2.9	(−)2.8	4.3	4.2
$^1C_4$	6.8	6.8	(−)2.4	(−)2.3	4.3	3.9
$^4C_1$	1.6	1.6	4.5	3.9	2.6	4.1
^2S_O	5.7	6.6	3.4	3.5	2.8	2.4
$^OS_2$	0.5	1.9	(−)2.6	(−)2.1	4.2	4.8

[a] For $^2J_{CC}$ the predicted values may be positive or negative, but only the absolute value can be measured.

0.6 to 1.2 Hz (Table 1). The two structures ***a*** and ***b***, described above, each fit the NMR data as well as the best linear combination of canonical conformations. This does not eliminate the possibility of a dynamic equilibrium between two or more conformations, but merely suggests that two individual conformations each can explain the data.

Mapping of Repeat Distance in the Conformational Space. Having analyzed how coupling constants vary in the conformational sphere, we turn to the question: Which area of ring conformational space would satisfy the experimentally determined helix parameters, n and h?[37,38] In addition to the sugar pucker, the interresidue torsions are also important in determining the helix symmetry, adding four degrees of freedom to the conformational space. To simplify the problem, we map the O1−O4 distance in $\theta-P_2$ space, and then focus on a limited number of conformations, for which interresidue torsional space can be searched for conformations that satisfy diffraction data. The O1−O4 distance is important, because the axial repeat length (h) observed for dermatan sulfate is long (9.2 Å for 8_3 helix, 9.4−9.7 Å for 2_1 helix, and 9.5 Å for 3_1 helix),[12−14] compared to that of heparin (8.2−8.7 Å),[45] even though the repeat unit backbone of dermatan sulfate (IdoA-α1,3-GalNAc) contains only 9 bonds compared to 10 for heparin (IdoA-α1,4-GlcNAc). When $^1C_4$ of α-L-iduronate (Table 1) is combined with $^4C_1$ of β-D-galactosamine,[12] no combinations of interresidue torsions can provide a helix of the observed axial repeat length for 2_1 and 3_1 helixes (Figure 6). Therefore, in general, short O1−O4 distances for iduronate conformations are inconsistent with the diffraction data for dermatan sulfate. Figure 5 shows the contour maps of the O1−O4 distance in the Northern and Southern hemispheres. The O1−O4 distance is much shorter (<4.5 Å) for $^1C_4$ ($\theta = 180°$) than for $^4C_1$ ($\theta = 0°$) (5.5 Å), and it is interesting that the variation in O1−O4 distance is highly asymmetric around the poles. For instance, iduronate conformations that map between $^1C_4$ and $^OS_2$ ($\theta = 90°$, $P_2 = 0°$) have O1−O4 distances, which increase significantly for θ values close to 180° ($^1C_4$), but for conformations that map between $^1C_4$ and ^2S_O ($\theta = 90°$, $P_2 = 180°$), the O1−O4 distance does not increase above 4.5 Å until θ is below 120° (Figure 5). This immediately suggests that if we search for a conformation close to the South pole ($^1C_4$) that is consistent with the long axial rises observed for dermatan sulfate fibers, the conformation should be perturbed in the direction of $^OS_2$ ($P_2 = 0°$). Otherwise, the conformation has to move all the way to the equator or to the Northern hemisphere. Thus, the ideal $^1C_4$ conformation cannot explain all the fiber diffraction data, but if one changes the conformation from $^1C_4$ in the direction of $^OS_2$, the calculated properties of the iduronate moiety correspond much better to the observed data for dermatan sulfate.

Having established the relationship between iduronate conformation and end-to-end distance in the entire ring conformational space, we then included the effect of interresidue torsions for a *limited* number of iduronate conformations. We fixed the iduronate ring in one of the six conformations (***a***, ***b***, $^4C_1$, $^1C_4$, ^2S_O, and $^OS_2$) and searched the entire 4-dimensional glycosidic torsion angle space for disaccharide conformations that satisfy each of the three observed helixes (2_1, 8_3, and 3_1). For each of the six iduronate ring conformations, we generated a $\phi1,\psi1$ and a $\phi2,\psi2$ map of the nonbonded energy of a dermatan sulfate oligosaccharide at the level of 5 kcal/mol, to represent the stereochemically accessible domain (Figure 6). The combinations of glycosidic torsion angles that satisfy experimental helixes for each iduronate conformation were then compared to the energy maps, and values that did not map within the stereochemically accessible domain were excluded. Finally, plots of the $\phi1,\psi1$ and $\phi2,\psi2$ maps for each iduronate conformation were prepared and the location of disaccharide conformations that satisfy the 2_1, 8_3, and 3_1 helixes, respectively, were indicated. From Figure 6, it is clear that the stereochemically accessible domain is very similar for all six iduronate conformations. This indicates that the general shape of the domain is determined by the nearest neighbor atoms (e.g., C2 and O5 of IdoA for the $\phi2,\psi2$ linkage), the positions of which are independent of iduronate ring conformation for a given value of glycosidic torsions. For iduronate structures ***b*** and $^1C_4$, only the 8_3 helix could be satisfied within the stereochemically accessible domain, and only at a few points. On the other hand, a wide range of combinations of glycosidic torsion angles lead to helical parameters that satisfy the 2_1, 8_3, and 3_1 helixes for the other four iduronate conformations. The $^4C_1$ conformation, despite having the longest O1−O4 distance (5.51 Å), does not have the widest range of values of glycosidic torsions that are

(45) Nieduszynski, I. A. *Polysaccharides—Topics in Structure and Morphology*; Atkins, E. D. T., Eds.; VCH: Weinheim, Germany, 1985; pp 107−139.

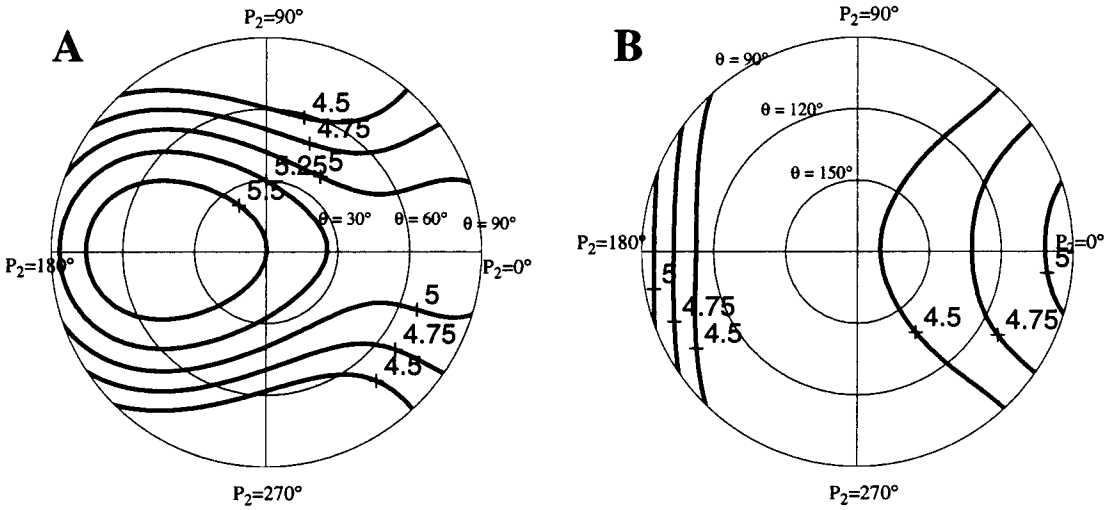

Figure 5. Mapping of the O1−O4 distance in iduronic acid ring conformational space. For each point in the conformational space, Cartesian coordinates for the ring atom glycosidic oxygens were generated as described. The O1−O4 distance is contoured at 4.50, 4.75, 5.00, 5.25, and 5.50 Å, in a 2D-projection of the conformational space, similar to Figure 2 (Figure 5A is the Northern and Figure 5B the Southern hemisphere).

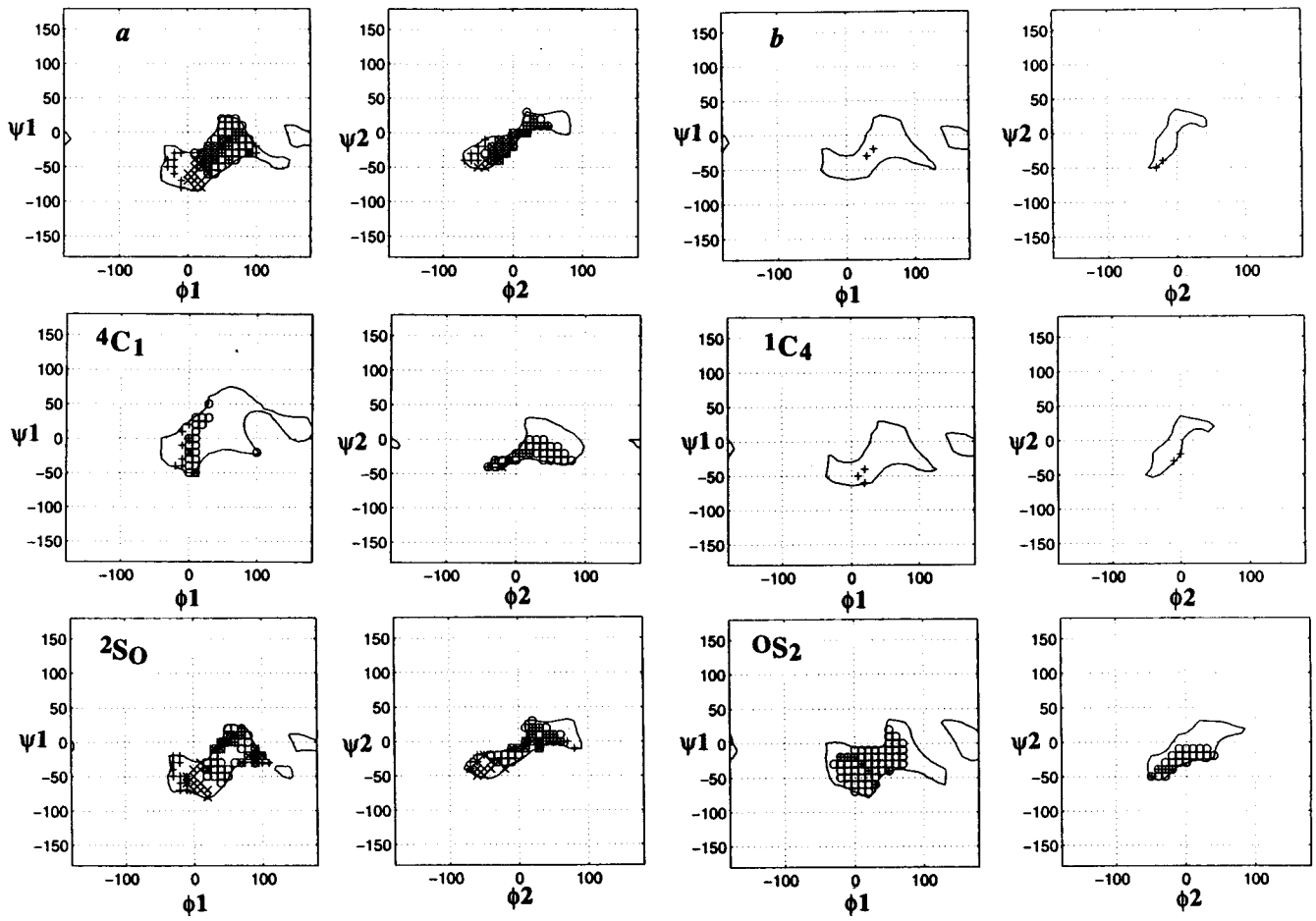

Figure 6. Mapping of the combinations of glycosidic torsions, which satisfy one of the helices (either 2_1 (○), 8_3 (+), or 3_1 (×)), and which fall within the stereochemically accessible domain ($E_{\text{non-bonded}} \leq 5$ kcal/mol indicated with contour). For each conformation of iduronate (***a***, ***b***, $^4C_1$, $^1C_4$, ^2S_O, and $^OS_2$), two plots are shown, ϕ_1,ψ_1 and ϕ_2,ψ_2. For each of the energy plots (e.g. ϕ_1,ψ_1), the values of the other set of glycosidic torsions (ϕ_2,ψ_2) are kept constant close to the center of the stereochemically accessible domain. For the calculation of helix symmetry, each point that satisfies a given helix is defined by all four glycosidic torsions. The points that are indicated in one plot (e.g. ϕ_1,ψ_1) are thus linked to a point in the other plot (ϕ_2,ψ_2). The glycosidic torsions are defined as ϕ_1 = H1′−C1′−O1′−C4, ψ_1 = C1′−O1′−C4−H4, ϕ_2 = H1−C1−O1−C3′, and ψ_2 = C1−O1−C3′−H3′ (see Figure 1).

consistent with the helix parameters. In fact, only $\phi1$ values in a narrow range from −20° to 30° (except for a single point at $\phi1,\psi1 = 100,-20$) are consistent with one of the three helixes. It appears that a O1−O4 distance of 5 Å (e.g., for structures ***a***, ^2S_O, and $^OS_2$) results in the largest range of glycosidic torsions that can satisfy the diffraction data. Thus, for a given helix symmetry, these iduronate conformations may be entropically favored compared to ***b***, $^1C_4$, and $^4C_1$.

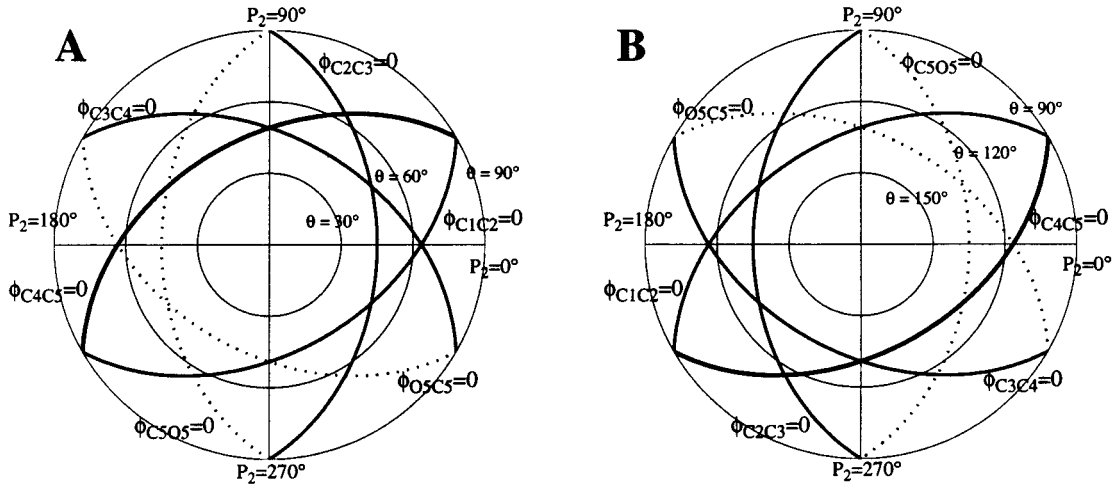

Figure 7. Mapping of eclipsed intraring torsion angles in a 2D-projection of the iduronic acid ring conformational space, similar to Figure 2. The contours of ϕ_{C1C2}, ϕ_{C2C3}, and ϕ_{C3C4} equal to zero are shown in regular lines. ϕ_{C5O5} and ϕ_{O5C1} equal to zero are shown in broken lines, to indicate low energy barriers to interconversion. ϕ_{C4C5} equal to zero is shown with a thick line, to indicate a large barrier to interconversion. Figure 7A is the Northern and Figure 7B the Southern hemisphere.

With the iduronate monomers in the conformation of structure ***b***, which satisfied NMR data[15] and had a somewhat longer O1−O4 distance than the ideal $^1C_4$ ($\theta = 180°$), only the shortest helical rise (9.2 Å for 8_3 helix) could be explained satisfactorily. However, all three helixes (2_1, 3_1, and 8_3) could be satisfied for structure ***a***, which also fits the NMR data for dermatan sulfate well. Winter et al. determined solid-state 1D-^{13}C NMR data and diffraction data for *the same* dermatan sulfate sample.[16] They found that the NMR data were similar to solution NMR data obtained previously,[46] and that the diffraction pattern was consistent only with 8_3 symmetry, not with 2_1 or 3_1 symmetry. Therefore, the iduronic acid of their dermatan sulfate sample could be in a conformation similar to either structure ***a*** or ***b*** we describe here. Our results, however, indicate that only structure ***a***, or conformations closer to the equator or at the Northern hemisphere, can explain the 2-fold and 3-fold helixes observed for dermatan sulfate. Thus, it is of interest to analyze how conformations on different hemispheres can interconvert.

Paths of Interconversion. When a pyranose ring changes from one domain in conformational space to another, either due to a change in environment or due to random thermal motion, it passes through a range of intermediate states, here called the path of interconversion. The literature on α-L-iduronate in dermatan sulfate and heparin has recently invoked a dynamic conformational equilibrium between several local minimum points in conformational space.[4,8,10,44] Addressing the issues of kinetics or pathways of interconversion quantitatively is very difficult because of the necessity to model the *absolute* energies of interconversion accurately. However, one can qualitatively investigate the most likely path of interconversion by a simple evaluation of the relative magnitude of the energy barriers of different paths. To change from a polar conformation to an equatorial conformation, three endocyclic torsion angles must pass through the eclipsed form. This is associated with an energy barrier, partly due to steric overlap between exocyclic groups, which will also be eclipsed.[47] This energy barrier will be lowest if the eclipsed endocyclic torsion angle involves the unsubstituted ring oxygen (ϕ_{C5O5} and ϕ_{O5C1}). Thus, the most likely path of interconversion is the one where the fewest substituted endotorsions have to pass through eclipsed forms. Further, ϕ_{C4C5} is the only endotorsion for which two heavy exocyclic groups (O4 and C6) are eclipsed when the endotorsion is eclipsed. Thus, eclipsed ϕ_{C4C5} represents an extra high energy barrier for interconversion. In Figure 7 the contours of eclipsed endotorsions are mapped with broken lines indicating the lower energy barrier associated with unsubstituted endotorsions being eclipsed and fat lines indicating the high energy barrier for endotorsion ϕ_{C4C5} being eclipsed. The most likely path of interconversion goes from $^1C_4$ at the South pole to a region between $^OS_2$ (90°, 0°) and $^3S_1$ (90°, 60°) at the equator, or from $^4C_1$ at the North pole to a region between ^2S_O (90°, 180°) and $^1S_3$ (90°, 240°) at the equator. It is anticipated that interconversions between equatorial states are faster than interconversions between poles and the equator, because they maintain bond lengths and bond angles unstrained, as opposed to interconversions between poles and the equator.[48] This analysis indicates that there is a special relationship between $^OS_2/^3S_1$ and $^1C_4$ and between $^2S_O/^1S_3$ and $^4C_1$, in that these skew-boat forms represent bridging points for interconversion between equatorial and polar conformations of iduronate.

Molecular dynamics (MD) represents a more sophisticated approach to investigate conformational dynamics. For α-L-iduronate, Forster and Mulloy[4] performed 200 ps MD calculations from three different starting conformations ($^1C_4$, $^4C_1$, and ^2S_O). For the two chair forms, the calculations showed considerable flexibility around the poles, with the Cremer−Pople azimuthal angle (θ) varying by 30°, and for the skew-boat, there was extensive pseudorotation along the equator, and one conversion to the polar $^4C_1$ conformation after 171 ps.[4] Engelsen et al.[3] performed similar simulations for ethyl-β-lactoside, and observed a shift from the pole to the equator during a 200 ps simulation. These MD calculations suggest that the equatorial interconversion is more facile than equatorial to polar interconversion and, in the case of iduronate, that the shift from equatorial conformation to $^4C_1$ occurs when $P_2 = 180°$ (Cremer−Pople $\phi_2 = 150°$) corresponding to the ^2S_O conformation.[4] This supports the conclusion of our analysis that an equatorial conformation close to the skew-boat ^2S_O may be a the starting point for the interconversion path between the equator and the North pole ($^4C_1$).

(46) Hamer, G. K.; Perlin, A. S. *Carbohydr. Res.* **1976**, *49*, 37−48.
(47) Morrison, R. T.; Boyd, R. N. *Organic Chemistry*; Allyn and Bacon: Boston, MA, 1973.
(48) Crippen, G. M. *J. Comput. Chem.* **1992**, *13*, 351−361.

Conclusions and Significance

We find that the torsion angle formalism introduced by Haasnoot[5] is advantageous due to the conformational significance of the torsion angles that are used as the basis for the internal coordinates, and due to the ease of calculating internal coordinates from a point on the conformational sphere. Both the Haasnoot and the Cremer−Pople formalisms allow deviations from canonical conformations to be described explicitly with the spherical parameters (Q, θ, and P_2/ϕ_2), without providing atomic coordinates. The conformational mapping and plotting techniques presented here represent a new approach to relate individual sugar pucker conformation to calculable parameters, and visualize the domains of good fit to experimental data. It offers a rapid way of mapping a given parameter in a continuous conformational space and eliminate geometries that are not accessible or do not fit physical data. Also, it provides a pictorial description of the pyranose ring conformational space, which can be useful in appreciating the problems of assessing ring flexibility. This approach to analysis of pyranose ring flexibility may be extended to conformational mapping of any other physical data that can be explicitly modeled from internal coordinates, such as NOE data or C−C and C−H couplings, and can thus be useful for identifying a single conformation that satisfies several sets of data. Applied to other hexoses, it may help identify the role of ring flexibility for carbohydrate-binding proteins or for enzymatic conversion of carbohydrates.

We have used the torsion angle formalism[5] to continuously map, in conformational space, calculable data of experimentally observable quantities. This graphical mapping technique, based on a two-dimensional projection of the spherical conformational space, was used to analyze the experimental data for the α-L-iduronate ring in dermatan sulfate. Earlier interpretation of the experimental data (X-ray fiber diffraction and NMR) for dermatan sulfate, using energy minimized conformations, led to conflicting results for the iduronate moiety. The solid-state and solution NMR were identical for dermatan sulfate in the 8_3 helix state, indicating that one conformational state should explain both NMR and diffraction data.[16] The mapping technique enables a combined analysis of the physical data that applies to this iduronate ring conformation, and allows identification of two possible solutions. Both the solution NMR data and the diffraction data for the 8_3 helix can be explained individually by two stereochemically accessible iduronate structures. One conformation (structure ***b***) is located close to $^1C_4$ on the most likely path of interconversion between the $^1C_4$ polar conformation and the $^OS_2$ equatorial conformation; the other conformation (structure ***a***) is located close to ^2S_O and has equatorial O2−O3 enolate suggesting high susceptibility to periodate oxidation, consistent with observations.[17] Only structure ***a*** or different domains in conformational space, such as the canonical ^2S_O and $^4C_1$ conformations, are consistent with the 2-fold and 3-fold helixes observed at different conditions.[12−14] We suggest that the iduronate residue is inherently flexible, manifested in the many possible conformers we found in our exhaustive search.[20] Thus, the ring conformation state may be best characterized as a broad, stereochemically accessible minimum, with the location of the global minimum being determined by environmental parameters. This is supported by crystal structures of basic fibroblast growth factor (bFGF) bound to heparin-like oligosaccharides;[18,19] the different ligands bind to the same site on the growth factor, however, the ring conformation of their iduronic acids varies considerably. The iduronic acid of synthetic di- and trisaccharides appeared as a $^4C_1$ conformer (Q, θ, P_2) = (60°, 3°, 97°),[18] as opposed to the two iduronic acids of a heparin-derived hexasaccharide, which were in ^2S_O (Q, θ, P_2) = (70°, 91°, 187°) and $^1C_4$ (Q, θ, P_2) = (58°, 170°, 156°) conformations, respectively.[19] Thus, the conformational flexibility of iduronate allows it to attain a variety of conformations when bound to bFGF, a property that is highly unusual for pyranoses. Members of the glycosaminoglycan (GAG) family of acidic polysaccharides, such as heparin, heparan sulfate, and dermatan sulfate, contain iduronate. These GAGs are ubiquitous components of the extracellular matrix. Among other functions,[49] they bind to proteins and modulate their activity,[9,50,51] which has implications in signal transduction,[52] in the coagulation cascade,[53] and in leukocyte trafficking.[54] These GAG−protein interactions often are specific for sequences of modified disaccharide residues of the GAG. Further, the ring conformational flexibility of iduronate, the modeling of which we have addressed in this paper, may play an important role in determining specificity of GAG−protein binding.

Acknowledgment. We greatly appreciate financial support from National Science Foundation through the Biotechnology Process Engineering Center at MIT and from the National Institutes of Health (GM 25810 and GM 57070). We are grateful to Biosym Technologies and Biosym-MSI for making available at the Department of Chemical Engineering at MIT the Insight II and Discover software packages, and to Dr. Pattabiraman for providing the NANDH program. Parts of this work were presented at the 211th National Meeting of the American Chemical Society.

JA972185O

(49) Poole, A. R. *Biochem. J.* **1986**, *236*, 1−14.
(50) Jackson, R. L.; Busch, S. J.; Cardin, A. D. *Physiol. Rev.* **1991**, *71*, 481−539.
(51) Varki, A. *Glycobiology* **1993**, *3*, 97−130.
(52) Rapraeger, A. C. *Curr. Op. Cell Biol.* **1993**, *5*, 844−853.
(53) Bourin, M.-C.; Lindahl, U. *Biochem. J.* **1993**, *289*, 313−330.
(54) Norgard-Sumnicht, K. E.; Varki, N. M.; Varki, A. *Science* **1993**, *261*, 480−483.